RSC Advances

ROYAL SOCIETY OF CHEMISTRY

www.rsc.org/advances

Realization of Highly-Dense Al$_2$O$_3$ Gas Barrier for Top-emitting Organic Light-Emitting Diodes by Atomic Layer Deposition

Min Li [a], Dongyu Gao [b], Shuo Li [c], Zhongwei Zhou [a], Jianhua Zou [a], Hong Tao [a], Lei Wang [a], Miao Xu [a*], Junbiao Peng [a*]

[a] Institute of Polymer Optoelectronic Materials and Devices, State Key Laboratory of Luminescent Materials and Devices, South China University of Technology, Guangzhou 510640, PR China

[b] Guangzhou New Vision Optoelectronic Co., Ltd., Guangzhou 510530, PR China

[c] Aalto University, Department of Micro- and Nanosciences, Tietotie 3, 02150 Espoo, Finland

ABSTRACT: This paper prepared Al$_2$O$_3$ film by the method of atomic layer deposition (ALD) as the thin film encapsulation technology for top-emitting organic light-emitting diodes (TE-OLED). Time-of-flight secondary ion mass spectrometry (TOF-SIMS), X-Ray Reflectometry (XRR) and X-ray photoelectron spectroscopy (XPS) are used to analyze the effect of different chemical precursors and behavioral factors on the performance of Al$_2$O$_3$ thin films. The analyses disclosed that Al$_2$O$_3$ films prepared with trimethylaluminum (TMA) and H$_2$O (TMA+H$_2$O) process contained more unreacted −CH$_3$ groups, and the films with TMA+O$_3$ process show a large number of carbon-based impurity. However, the Al$_2$O$_3$ films prepared by using H$_2$O and O$_3$ in turn in a deposition cycle as oxygen sources exhibited higher density and purity, leading to a superior water vapor transmission rate (WVTR) as low as 5.43×10$^{−5}$ g/m^2/day estimated by Calcium (Ca) corrosion method at 40℃/100%. The TE-OLED with Al$_2$O$_3$ (TMA+H$_2$O+O$_3$) thin film as encapsulated layer has longer lifetimes, and produces no black spots under operational times up to 400 hours.

1. Introduction

A big challenge for the organic light-emitting diodes (OLED) development in widespread application is their vulnerability to ambient moisture and oxygen.[1-3] The requirement of water vapor transmission rate (WVTR) in OLED is more rigorous than those of any other packaging application, that needs to be less than 10$^{−6}$ g/m^2/day.[4] Glass to glass encapsulation technology is the state-of-the-art scheme for organic electronics. But thin film encapsulation (TFE) technique is indispensable for

realization of flexible OLED. Nowadays, atomic layer deposition (ALD) is considered as the most promising method to produce gas barrier for encapsulation of OLEDs, because of its special features, such as low-temperature process, conformal film deposition, pinhole-free, high quality layer, and excellent uniformity.[5-8]

In the deposition of gas barrier layers by ALD, aluminum oxide (Al_2O_3) is the most investigated and used materials in the field of thin film encapsulation. The deposition is usually performed using TMA and H_2O as precursors and reactants, which is considered as an ideal self-limiting process for ALD growth. Since the first report by G. S. Higashi and C. G. Fleming in 1989,[9] the low temperature process of Al_2O_3 has been extensively studied and characterized in the details of precursor chemistry and performance evaluation for TFE application.[10,11] Besides water, ethylene glycol and ozone or oxygen plasma have been widely used as oxygen reactants with TMA to obtain densely film.[12-14] Most recently, Duan's group have optimized the pumping gas time (PGT) to purge the excess H_2O or O_3 as a way to fabricate Al_2O_3 gas barrier with lower WVTR.[15] In addition, Al_2O_3 film as the building blocks was employed in the laminated structure for configuration of highly impermeable gas barrier, such as Al_2O_3/TiO_2 and Al_2O_3/ZrO_2 stacked structure.[16,17]

In this study, we investigate the gas barrier performance of ALD thin film encapsulations with a single layer of Al_2O_3. For this investigation, the influence of gas species and its way of import into the substrate on barrier properties is examined. The highlight of this work is that with H_2O and O_3 as basic reactants in ALD process, Al_2O_3 film with lower WVTR can be achieved by dividing the introduction of oxygen source into two steps, that is to say, H_2O reactant was firstly pulsed into the substrate with TMA chemisorbed, and then O_3 was pulsed into chamber for further reacted with the residual methyl group in TMA. This ternary reaction system (TMA+H_2O+O_3) can realize an Al_2O_3 film with high density, which achieves a superior WVTR as low as 5.43×10^{-5} $g/m^2/day$. Additionally, the deposition rate of this reaction can be greatly improved. The top-emitting OLED (TE-OLED) encapsulated with ternary reacted Al_2O_3 exhibits an excellent storage property that without any visible black spot growth under the particular conditions (temperature=40 °C, humidity=100%).

2. Experimental procedures

For this study, Al_2O_3 layer was grown at 80 °C with BENEQ TFS500 system, using TMA, H_2O, and O_3 as precursor gases. Ozone precursor was produced by an ozone generator BMT Messtechnik 803N using oxygen and catalytic nitrogen to gain approximately 8 g/h ozone production. In this experiment, we fabricated three kinds of Al_2O_3 thin film as a comparison to identify the role of oxidizing precursors reacted with TMA. Film A, B, and C was donated as the Al_2O_3 film fabricated with TMA+O_3, TMA+H_2O, and TMA+H_2O+O_3 precursors. The pulse time for TMA and H_2O was fixed at 0.25 s, and pulse durations of O_3 were varied from 0 to 50 s. The purge time for TMA, H_2O, and O_3 was kept the same as 10.0 s. In the ternary reaction systems, the import of O_3 precursor was following the completion of H_2O purge. The schematic illustration of technical flow process was shown in Fig. 1.
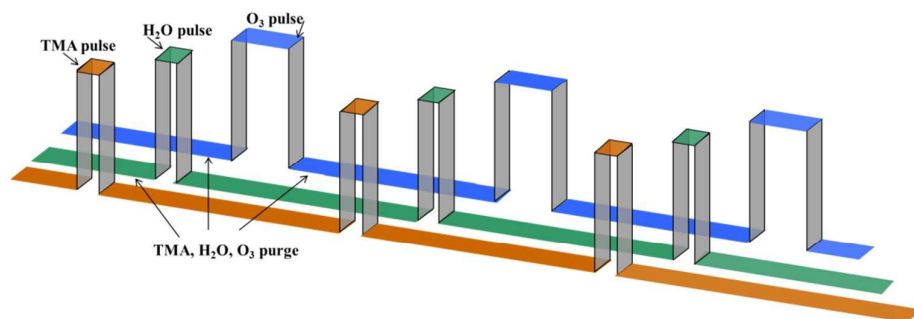

Fig. 1 Illustration of technical flow process for Al_2O_3 film with TMA+H_2O+O_3 ternary reacted system.

The film thickness and reflective index of the deposited films were measured by spectroscopy ellipsometry (SE). The X-Ray Reflectometry (XRR, Bruker D8 advance diffractometer) as an effective approach to evaluate the film density was carried out. The dielectric performance was characterized by a semiconductor parameter analyzer (Agilent B1500A). For the film with different oxygen reactants, the secondary ion mass spectroscope (SIMS, PHYSICAL ELECTRONICS, TRIFT II Model 2100) was measured to confirm the incorporation of elements and chemical group in the Al_2O_3 films. The chemical bonding states on the bulk Al_2O_3 films were observed with an x-ray photoelectron spectroscopy (XPS, Thermo, ESCALAB 250). The film interfacial property of Al_2O_3 used as barrier film was investigated by high-resolution

transmission electron microscopy (HR-TEM, JEOL, JEM-2100F).

In this study, the structure of the green TE-OLED was Glass/Ag(100 nm)/IZO(7.6 nm)/MeO-TPD:F4-TCNQ(156 nm), 4 wt%) /NPB (20 nm)/VOM1511:GD-5 (40 nm)/Bebq2: (25 nm)/LiF(1 nm)/Mg:Ag (9:2, mass ratio, 15 nm)/ZnSe(24 nm), Where MeOTPD: F4-TCNQ is tetrafluoro-tetracyanoqino dimethane doped into N,N,N,N-tetrakis(4-methoxyphenyl)-benzidine as hole injection layer (HIL), NPB is N,N-Bis(naphthalen-1-yl)-N,N-bis(phenyl)benzidine as hole transport layer (HTL), VOM1511:GD-5 is green emitting layer, Bebq2 is bis(10-hydroxybenzo[h]quinolinato)beryllium complex as electron transport layer (ETL) and LiF/Mg:Ag is transparent cathode. ZnSe is capping layer. MeO-TPD, F4-TCNQ, NPB, Bebq2 were home-made, VOM1511 and GD-5 were commercial materials and purchased from Visionox Corporation and ZnSe is purchased from Alfa Aesar, respectively.

3. Results and discussion

In order to characterize the growth mechanism of the Al_2O_3 films, the thickness variations with different oxidizing reactants were measured using a spectroscopic ellipsometer. The films were prepared by using 500 cycles of ALD deposition grown on a Si wafer. The results shows the growth rate of the TMA+H_2O and TMA+O_3 Al_2O_3 films was approximately 0.796 Å/cycle and 1.189 Å/cycle, which means that O_3 is more effective to acquire a thicker Al_2O_3 films than H_2O during one cycle, owning to the stronger oxidizing capacity of O_3 gas precursor.[18] Meanwhile, As increasing the pulse time of H_2O from 0.25 s to 2.0 s (the data was not shown here) for TMA+H_2O Al_2O_3, the film growth rate will be increased gradually but with an almost saturated value as 0.943 Å/cycle, indicating that the H_2O reactants could not completely exhaust the molecule group in TMA precursor at the deposition temperature. But as the introduction of O_3 after H_2O in a cycle process, the growth rate started to increase rapidly. As shown in Fig. 2, the increment of time for the O_3 import will sharply improve the reaction rate, and the value is 1.157 and 1.356 Å/cycle for 2 s and 30 s O_3 pulse time. The improvement of deposition rate indicates that the residual TMA precursor in the TMA+H_2O process at the low processing

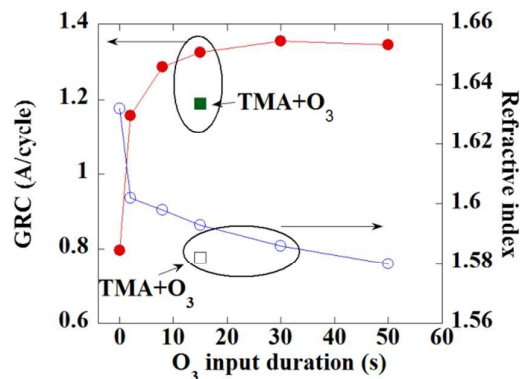temperature can be consumed by a subsequent O_3 cycle.

Fig. 2 The film growth rate per cycle (GRC) and refractive index of Al_2O_3 film fabricated with

different oxygen reactants.

The refractive index measured from spectroscopic ellipsometers are 1.632 and 1.582 for TMA+H_2O and TMA+O_3 Al_2O_3 films, respectively, which is similar with previous reports. [19] But as introducing the O_3 after H_2O precursor in the reaction system, the refractive index gradually dropped from 1.602 to 1.580 as increasing O_3 pulsing time from 2.0 s to 50.0 s. Conventionally，the decrease of refractive index implies the degradation of density of the film. And the density of barrier films would influence the barrier performance crucially.

To further confirm film density of Al_2O_3 films, the XRR as an effective approach to evaluate the density was carried out. Through the critical angle analysis by XRR measurement, the fitting value of density could be obtained, as shown in Fig. 3(a). The XRR density for Al_2O_3 films deposited with TMA+H_2O and TMA+O_3 is 2.95 g/cm^3 and 2.80 g/cm^3. The maximum XRR density (3.00 g/cm^3) is observed for the film with the introduction of ozone after H_2O reactants, implying that the decrease of refractive index with adding ozone pulses in TMA+H_2O process cannot be explained by the decreased density of Al_2O_3 films. The lowest XRR density is obtained in TMA+O_3 Al_2O_3 film, which is due to the nature of ozone species in the specific temperature. The number of effective radical generated by ozone at low temperature is inadequate, accompanying with the traits of lower ozone concentration and short radical lifetimes. This determines the ozone can't effectively penetrate into the internal

groups in every mono-molecular deposition to form a dense Al_2O_3 framework. As another important clue, Fig. 3(b) shows the leakage behavior of Al_2O_3 dielectrics with different oxygen reactant. The leakage current decreases as the H_2O and O_3 precursor introduces into chamber by step due to more complete reaction by the more drastic oxygen species. The test results prove that $TMA+H_2O+O_3$ Al_2O_3 show a superior dielectric property as comparison to the single reactant of H_2O or O_3. Hence film density or quality of Al_2O_3 increases with the additional introduction of ozone in the process. This improvement could be understood as a compaction of the Al_2O_3 film through removal of holes/voids as well as a reduction of hydrogen impurities.
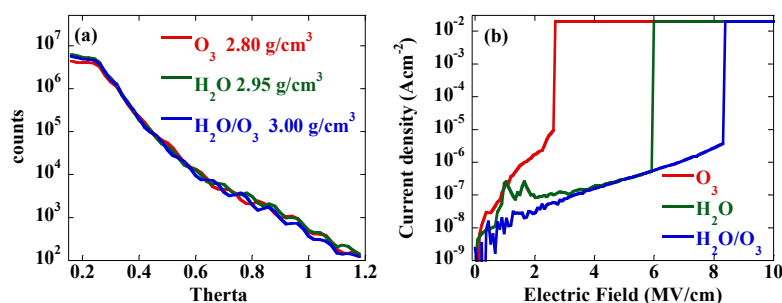

Fig. 3 (a) The film density measured by XRR and (b) insulator characteristic of Al_2O_3 film fabricated with different oxygen reactants.

For the films with different gas precursors, the TOF-SIMS was measured to confirm the residual unreacted methyl and the incorporation of hydrogen related species in the Al_2O_3 films. As seen in Fig. 4, the $TMA+O_3$ Al_2O_3 film shows a lowest $-CH_3$ group in the internal film, resulting from the fact that the ozone has better oxidation property. But in the traditional $TMA+H_2O$ Al_2O_3 film, a larger amount of $-CH_3$ was embedded, indicating that H_2O reactants could not fully exhaust the group in the every TMA pulsing cycle at the low process temperature. But the following introduced O_3 with stronger oxidizing capacity could effectively consume part of the unreacted $-CH_3$ group, thus making the film more densely as manifested in the $TMA+H_2O+O_3$ Al_2O_3. Moreover, the $-OH$ and $-H$ species survived in the $TMA+H_2O+O_3$ Al_2O_3 film was reduced as compared to $TMA+H_2O$ Al_2O_3. These species are speculated to be one of the reasons for lower water and oxygen permeability, which seems to speed up the formation of permeable channel for water

and oxygen molecules. The lower concentration of −OH and −H species would be more popularized for prolonging the diffusion paths of permeated molecules.

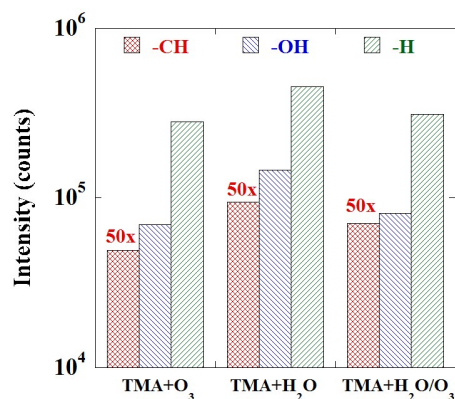**Fig. 4** TOF-SIMS results of –CH$_3$,–OH, and–H group in Al$_2$O$_3$ film with different oxygen reactants, and the value of –CH$_3$ content amplified by 50 times as comparison.

The chemical composition and bonding states of the Al$_2$O$_3$ film fabricated with different precursors were investigated in detail of the C1s, O1s and Al2p core level spectra with x-ray photoelectron spectroscopy. To avoid surface contamination of the samples during the XPS measurements, the films were sputtered off the extreme surface of samples exposed to ambient air. Fig. 5(a)–(c) shows the high resolution of C1s core level spectra for Al$_2$O$_3$ films. The C1s core level was fitted with two peaks assigned to –CH$_2$–CH$_2$– bonds (C1sA peak set at 285.3 ± 0.1 eV), C=O bonds (carboxyl groups and carbonates, C1sB peak at 290.4 ± 0.1 eV).[20] As shown in Fig. 5(a), it can be seen that a lot of C=O bonds survived in the Al$_2$O$_3$ film, owning to the stronger oxidizing capacity of the ozone with the result of methyl oxidation. The carbonate related impurity C=O induced by ozone process may lead to the generation of irregular Al-O-Al bridge, ultimately deteriorating the density of Al$_2$O$_3$ film proven by XRR measurement. The inferior density would lead directly to a poor gas barrier performance. But, as shown in Fig. 5(b), the absence of carboxyl-related signal and a smaller peak area indicates no carbonate impurities and less carbon residual in the TMA+H$_2$O film. On the other hand, interestingly, the amount of C=O bonds and the total carbon residual remarkable increased by inducing an extra following ozone pulse in the TMA+H$_2$O+O$_3$ ternary reacted system. The existence of C=O bonds can be

explained by the reaction between residual −CH$_3$ groups, that could not be triggered during H$_2$O pulse, and the following O$_3$ precursors. Moreover, the increasing content of carbon compared with TMA+H$_2$O process should be attributed to the residual of oxidation functional groups (hydroxyl, epoxide etc.) induced by O$_3$ precursor. These residual could further react with –CH$_3$ groups in the following cycle of overdosed TMA precursor, thus leaving carbon-related impurities in the Al$_2$O$_3$ film. The last required a bit of explanation that the reduction of reflective index obtained in Fig.2 can be well explained by this introduction of carbon related impurity in the ternary reacted Al$_2$O$_3$ film, but it seems not to degrade the film density.
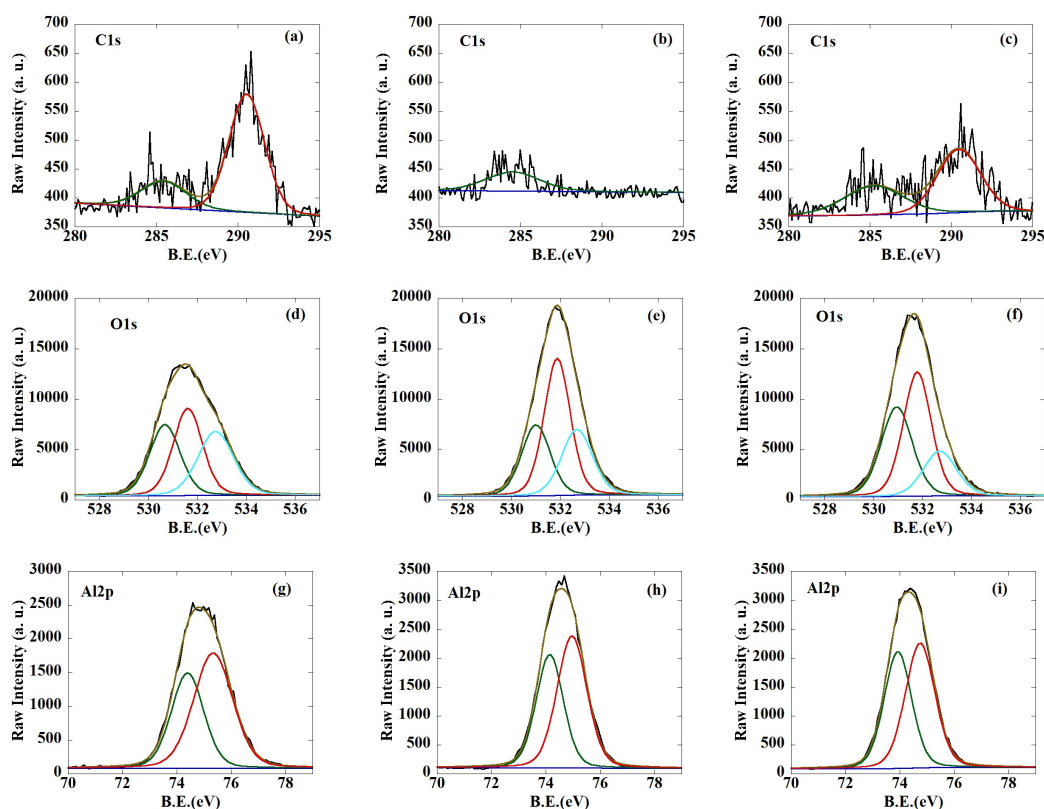

Fig. 5 The XPS spectra of C1s, O1s and Al2p in (a, d, g) TMA+O$_3$, (b, e, h) TMA+H$_2$O, and (c, f, i) TMA+H$_2$O+O$_3$ Al$_2$O$_3$ film.

The XPS survey spectra presented in Fig. 5 also show the high resolution O1s and Al2p core level spectra. Three peaks were used for fitting the O1s spectra as shown in Fig. 5(d)–(f). The main component (O1sA) at the BE of 530.8 ± 0.1 eV is attributed to the oxide ions of the alumina matrix. The O1sB peak observed at 531.7 ± 0.1 eV can be identified as oxygen vacancies or hydroxyl groups bonded with Al atom. The third

peak, O1sC at 532.7 ± 0.1 eV, is associated with the water molecules in the surface adsorption. [21] The TMA+O_3 Al_2O_3 film has a lower percentage of oxygen vacancies because of the strong oxidability generated by ozone, but more proportion of oxygen/water adsorption indicating the loose structure in the film. In the TMA+H_2O Al_2O_3 film, H_2O as the oxygen reactants cannot effectively form an ideal Al-O ratio leading to the existence of a certain amount of oxygen vacancies. However, the oxygen in lattice has greatly risen in the TMA+H_2O+O_3 ternary reacted system, while the adsorption of water on the surface reduces. This improvement occurred after the introduction of ozone, which makes the alumina structure more densification. For another, two peaks were used for fitting the Al2p core level spectra as shown in Fig. 5(g)–(i). The Al2pA peak at 74.1 ± 0.2 eV is assigned to the Al(III) ions of an oxide matrix. [22] The Al2pB peak at higher BE (75.0 ± 0.3 eV) is assigned to the Al(III) ions of an hydroxide matrix, as show in Table 1. The O:Al atomic ratio calculated with the O1sA and Al2pA components is1.42, 1.41, and 1.44 for the TMA+O_3, TMA+H_2O, and TMA+H_2O+O_3 Al_2O_3 samples. This means that the ternary reacted film is in more excellent agreement with the stoichiometry of Al_2O_3 (O:Al ratio of 1.5) and confirms the assignment of the O1sA and Al2p peaks. These peak information also shows that the binding energy of Al2pA peak in TMA+H_2O+O_3 film shift to lower position (73.9 eV) as comparison to the other two samples, indicating that the ternary reacted system is more essential for obtaining Al_2O_3 film with stoichiometry. This near-perfect structure will greatly strengthen the barrier performance of the TMA+H_2O+O_3 Al_2O_3 film. Moreover the amount of −OH and −H species will be significantly reduced owning to the ozone oxidation, which will finally enhance the film quality to repel the molecules diffusion. As a result, the TMA+H_2O+O_3 ternary reacted system will be more effective for realization an Al_2O_3 film with better barrier performance.

Table 1. The summary of the C1s, O1s, and Al2p peak properties for Al_2O_3 film.

Element	C1s		O1s			Al2p		Atomic
Precursor	C1sA	C1sB	O1sA	O1sB	O1sC	Al2pA	Al2pB	ratio(C/O/Al)
O_3	23.34%	76.66%	31.13%	36.29%	32.56%	40.64%	50.36%	2.01/57.5/40.49

| H$_2$O | 100.00% | 0.00% | 26.61% | 46.85% | 26.55% | 43.86% | 56.14% | 0.41/58.27/41.32 |
| H$_2$O/O$_3$ | 40.01% | 59.99% | 35.97% | 44.71% | 19.31% | 46.44% | 53.56% | 0.90/58.49/40.62 |

The film structure of Al$_2$O$_3$ layer used as barrier film in TFE structure was investigated by high-resolution transmission electron microscopy (HR-TEM). The four layers of Al$_2$O$_3$ were continuously deposited into the glass substrate with the sequence as TMA+H$_2$O+O$_3$, TMA+O$_3$, TMA+H$_2$O, and TMA+H$_2$O+O$_3$ based Al$_2$O$_3$ film. In this measurement, our starting point is to consider the quality difference of bulk Al$_2$O$_3$ film that fabricated with variable oxygen reactants, while slightly having shed light on the influence of surface properties that induce the initial grown film inconsistent on another surface. Fig. 6 shows that the interface between the adjacent layers of any two of these materials. Especially, the HR-TEM images clearly show that the TMA+O$_3$ Al$_2$O$_3$ film is quite different from the two other films. Experimental facts demonstrate that the contrast ratio of electron image depends on the directions of incident electron beam relative to that of crystals, which exhibits a lower film density. Therefore, the influence of TMA+O$_3$ Al$_2$O$_3$ film structures on the performance of gas-diffusion barrier can be included as one of the main causes. In other respect, the bulk characteristic between the TMA+H$_2$O+O$_3$ and TMA+H$_2$O Al$_2$O$_3$ is not very obvious, which can be also manifested in XRR measurement that have a close value of film density.
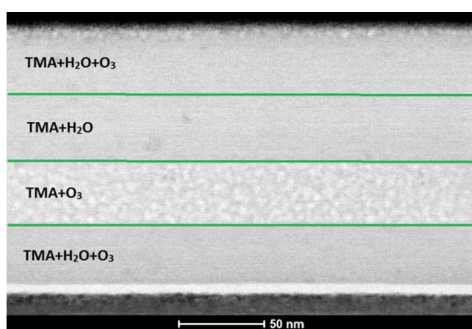

Fig. 6 The interface characteristic of Al$_2$O$_3$ film with variable oxygen reactants.

The WVTR measurements were carried out to evaluate the gas permeability of the Al$_2$O$_3$ film by using traditional calcium (Ca) corrosion method, which involves a Ca sensor at 40 °C and 100% RH. The 200-nm-thick Ca film with length/width (L/W)

as 10/20 mm was deposited on the patterned titanium electrodes (100 nm) with shape

of two narrow bars. The electrical measurements were performed using two electrodes

connected by SMU probe to the Keithley 2400 source meter. It is assumed that the Ca

film follows a laterally homogeneous corrosion during the erosion induced by the

water or oxygen molecule, as a result we can see that the amount of calcium left exists

a directly proportional relationship between calcium left and current measured. The

WVTR value was determined using the following equation:[23]

$$WVTR(g/m^2/day) = -n\delta_{ca}\rho_{ca}\frac{d(G)}{d(t)}\frac{L}{W}\frac{M(H_2O)}{M(Ca)}\frac{Area(Ca)}{Area(Window)}$$

where d(G)/d(t) is the change of Ca conductance as a function of time, and the n is the

molar equivalent of the degradation reaction. In this equation, δ_{ca} and ρ_{ca} are the Ca

resistivity (3.4×10^{-8} Ω m) and density (1.55 g/cm^3), where M (H$_2$O) and M (Ca) are

the molar masses of water and Ca. According to the geometry of the experimental

setup, the ratio of the area of the Ca sensor to the area of the window for water

permeation is consistent.

As shown of the Ca test in Fig. 7, the WVTR value for TMA+O$_3$ Al$_2$O$_3$ film is

4.15×10^{-4} g/m^2/day, while it is 9.64×10^{-5} g/m^2/day for TMA+H$_2$O Al$_2$O$_3$ film. It

seems that the H$_2$O reactant is more effective than the O$_3$ to fabricate high quality

Al$_2$O$_3$ film, although the oxidizing capacity of O$_3$ is much stronger than H$_2$O. But in

the ternary reaction system of TMA+H$_2$O+O$_3$, the predicted permeation rate of the

Al$_2$O$_3$ film calculated from this equation was 5.43×10^{-5} g/m^2/day, which has a better

comparability to other single Al$_2$O$_3$ film. These results indicate that the O$_3$ oxidizing

gas precursor is not alone to affect the film properties of Al$_2$O$_3$ film and its barrier

performance, indicating that it is quite different from those of single source of oxygen

species; therefore, we speculate that the introduction of O$_3$ after H$_2$O oxidizing gas

precursors will be acted as an effective way to further react with TMA precursor that

combined with foramtion of a densely film, which seems to strengthen the resistance

of water and oxygen molecules. Actually the permeation mechanism and dynamic

penetration process of water and oxygen molecular in the Al$_2$O$_3$ film is more complex.

Therefore, much more in-depth investigation of this ternary reacted film is necessary

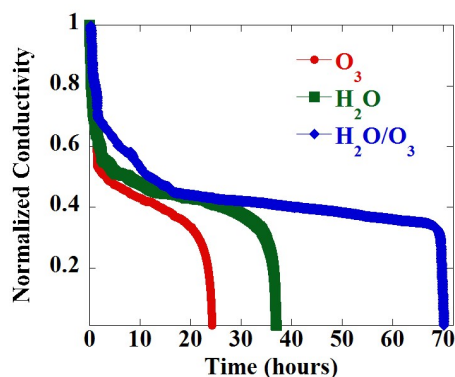when used in the thin film encapsulation technology.

Fig. 7 The normalized change of electrical conductance of Ca film with different Al_2O_3 as a

function of time.

The WVTR results have implied us that TFE structure based on $TMA+H_2O+O_3$ Al_2O_3 film may have excellent barrier properties when integrated on TE-OLEDs. The electroluminescent (EL) spectra of the encapsulated TE-OLEDs are firstly investigated. Fig. 8(a) shows that the EL spectra almost do not depend on the Al_2O_3 film architecture, which means that only slightly difference in EL spectra behavior between the devices with different precursors fabricated Al_2O_3 can be observed, indicating that the performance of the TE-OLEDs did not change appreciably in the process of thin-film encapsulation. To further verify the quality of the encapsulation layers, lifetime tests were performed. Fig. 8(b) shows the typical plots of normalized luminance versus operating time for TE-OLEDs in a nonstop constant-voltage mode with a starting luminance of 10 000 cd/m^2, which was measured in constant temperature and humidity using a luminance meter (KONICA MINOLTA CS-2000). For this study, the lifetime is defined as the decay time that the luminance decreases to 5 000 cd/m^2. Actually it is hard to make a distinction between internal mechanism of OLED degradation and external permeated water/oxygen degradation. Herein, we put forward the difference of Al_2O_3 films used in encapsulation with the assumption that the decay of the OLED itself is the same, so the luminance of the OLED device measured is merely a response of Al_2O_3 barrier performance for deterioration. As shown in Fig. 8(b), the luminance of the device with $TMA+H_2O+O_3$ Al_2O_3 encapsulation measured in oven deteriorated slower (with lifetime exceeding over 400

hours) than the elapsed luminance of the devices with TMA+O_3 or TMA+H_2O Al_2O_3 film capping, suggesting that the degradation induced by the H_2O or O_2 gases permeation into the TE-OLEDs was blocked off effectively in the ternary reacted film, which could be well attributed to the better performance of WVTR.
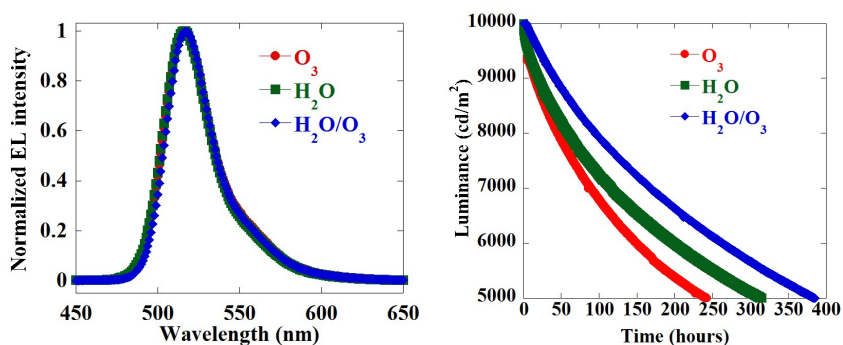

Fig. 8 (a) The EL spectra and (b) the TE-OLEDs luminescence versus continuous operation times for Al_2O_3 encapsulation with variable oxygen reactant.

The photography images of encapsulated TE-OLEDs stored in oven (40 °C, 100%) for 160 hours were recorded to verify the effect of TFE. The black spots are usually caused by cathode delamination due to reactions with ambient H_2O or O_2 gases. As shown in Fig. 9(c) and 9(f), the TMA+H_2O+O_3 Al_2O_3 film encapsulated OLEDs display a good image without obvious black spots. For further observation, the TE-OLEDs with H_2O or O_3 derived Al_2O_3 film encapsulated have been almost weakened with generation of many large-sized black spots, and proportion of the these black spots is thriving or having wider permeation paths to cause further damage. After being encapsulated with a densely Al_2O_3 barrier, the growth of initial black spots alleviates with a very slow rate, manifesting an excellent barrier performance for this kind of Al_2O_3 film.
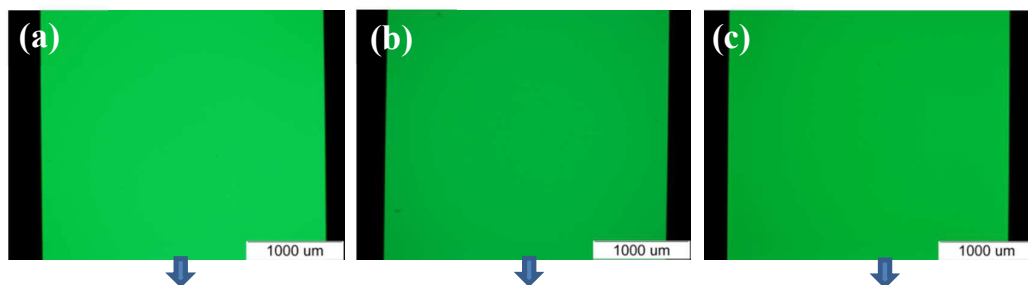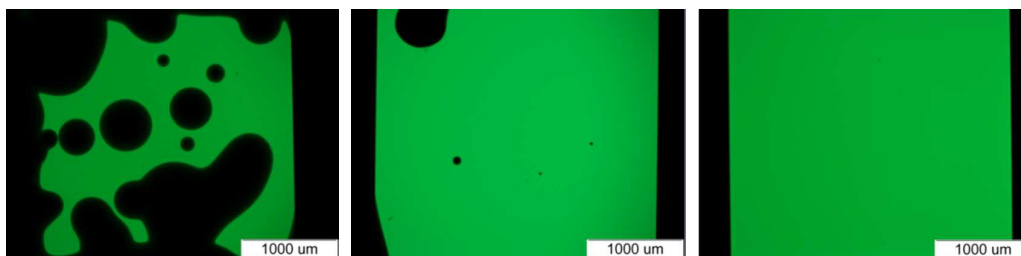
Fig. 9 Photography of three comparative TE-OLEDs. Before aging: (a) TMA+O$_3$, (b) TMA+H$_2$O,

(c) TMA+H$_2$O+O$_3$; After aging aged in oven for 160 hours: (d)-(f).

4. Conclusions

In summary, the barrier performance of Al$_2$O$_3$ film based on different oxygen reactants with TMA by use of atomic layer deposition was investigated. The TMA+H$_2$O+O$_3$ ternary reacted systems would lead to a more densely film structure as comparison to the single H$_2$O or O$_3$ based Al$_2$O$_3$. The TOF-SIMS results demonstrated that the H$_2$O precursor could not completely exhaust the −CH$_3$ group in TMA chemisorbed substrate if without the further import of O$_3$ gas, but the film with only O$_3$ as oxygen reactant (TMA+O$_3$) shows a certain amount of carbonate impurities, which will degrade the Al-O-Al bonding state. The produced Al$_2$O$_3$ thin film by TMA+H$_2$O+O$_3$ process shows an O/Al atomic ratio of 1.44 and deposition rate of 1.33 A/cycle, determining that it will has great advantages in the industrial production for future wearable/flexible displays when integrated in OLEDs thin film encapsulation.

Acknowledgements

References

(1) M. S. Weaver, L. A. Michalski, K. Rajan, M. A. Rothman, J. A. Silvernail, J. J. Brown, P. E.

Burrows, G. L. Graff, M. E. Gross and M. Zumhoff, *Appl. Phys. Lett.*, 2002, **81**, 2929−2931.

(2) R. Grover, R. Srivastava, M. N. Kamalasanan and D. S. Mehta, *RSC Adv.*, 2014, **4**, 10808.

(3) E. Gautier, A. Lorin, J. M. Nunzi, A. Schalchli, J. J. Benattar and D. Vital, *Appl. Phys. Lett.* 1996, **69**, 1071−1073.

(4) P. E. Burrows, G. L. Graff, M. E. Gross, P. M. Martin, M. Hall, E. Mast, C. C. Bonham, W. D. Bennett, L. A. Michalski, M. S. Weaver, J. J. Brown, D. Fogarty and L. S. Sapochak, *Proc. SPIE*, 2001, 75−83.

(5) A. A. Dameron, S. D. Davidson, B. B. Burton, P. F. Carcia, R. S. McLean and S. M. George, *J. Phys. Chem. C*, 2008, **112**, 4573.

(6) H. Kim, H. B. R. Lee and W. J. Maeng, *Thin Solid Films*, 2009, **517**, 2563−2580.

(7) J. Meyer, P. Goerrn, F. Bertram, S. Hamwi, T. Winkler, H. Johannes, H. T. Weimann, P. Hinze, T. Riedl and W. Kowalsky, *Adv. Mater.*, 2009, **21**, 1845−1849.

(8) O. Sneh, R. B. Clark-Phelps, A. R. Londergan, J. Winkler and T. E. Seidel, *Thin Solid Films*, 2002, **402**, 248−261.

(9) G. S. Higashi and C. G. Fleming, *Appl. Phys. Lett.*, 1989, **55**, 1963.

(10) M. D. Groner, F. H. Fabreguette, J. W. Elam and S. M. George, *Chem. Mater.*, 2004, **16**, 639−645.

(11) Y. G. Lee, Y.-H. Choi, I. S. Kee, H. S. Shim, Y. W. Jin, S. Lee, K. H. Koh and S. Lee, *Org. Electron.*, 2009, **10**, 1352−1355.

(12) X. Wang, Y. Duan, F. B. Sun, Y. Q. Yang, D. Yang, P. Chen,Y. H. Duan and Y. Zhao, *RSC Adv.*, 2014, **4**, 43850.

(13) Y.-Q. Yang, Y. Duan, P. Chen, F.-B. Sun, Y.-H. Duan, X. Wang and D. Yang, *J. Phys. Chem. C*, 2013, **117**, 20308−20312.

(14) D. Cao, X. Cheng, L. Zheng, D. Xu, Z. Wang, C. Xia, L. Shen, Y. Yu and D. Shen, *J. Vac. Sci. Technol. B*, 2015, **33**, 2166−2746.

(15) A. Singh, F. Nehm, L. Müller-Meskamp, C. Hoßbach, M. Albert, U. Schroeder, K. Leo and T. Mikolajick, *Org. Electron.*, 2014, **15**, 2587−2592.

(16) J. Meyer, H. Schmidt, W. Kowalsky, T. Riedl and A. Kahn, *Appl. Phys. Lett.*, 2010, **96**, 243308−243310.

(17) A. Singh, H. Klumbies, U. Schröder, L. Müller-Meskamp, M. Geidel, M. Knaut, C. Hoßbach,

M. Albert, K. Leo and T. Mikolajick, *Appl. Phys. Lett.*, 2013, **103**, 233302.

(18) Y. Q. Yang and Y. Duan, *J. Phys. Chem. C*, 2014, **118**, 18783−18787.

(19) Y.-Q. Yang, Y. Duan, Y.-H. Duan, X. Wang, P. Chen, D. Yang, F.-B. Sun and K.-W. Xue, *Org. Electron.*, 2014, **15**, 1120−1125.

(20) B. Díaz, E. Häköen, J. Swiatowska, V. Maurice, A. Seyeux, P. Marcus and M. Ritala, *Corros. Sci.*, 2011, **53**, 2168−2175.

(21) H. Jung, H. Jeon, H. Choi, G. Ham, S. Shin and H. Jeon, *J. Appl. Phys.*, 2014, **115**, 073502.

(22) L. H. Kim, K. Kim, S. Park, Y. J. Jeong, H. Kim, D. S. Chung, S. H. Kim and C. E. Park, *ACS Appl. Mater. Interfaces*, 2014, **6**, 6731−6738.

(23) Y. C. Han, C. Jang, K. J. Kim, K. C. Choi, K. Jung and B.-S. Bae, *Org. Electron.*, 2011, **12**, 609−613.